# Three-dimensional ray tracing of VLF waves in a magnetospheric environment containing a plasmaspheric plume

Lunjin Chen,[1] Jacob Bortnik,[1] Richard M. Thorne,[1] Richard B. Horne,[2] and Vania K. Jordanova[3]

Received 6 August 2009; revised 5 October 2009; accepted 8 October 2009; published 20 November 2009.

[1] A three dimensional ray tracing of whistler-mode chorus is performed in a realistic magnetosphere using the HOTRAY code. A variety of important propagation characteristics are revealed associated with azimuthal density gradients and a plasmaspheric plume. Specifically, whistler mode chorus originating from a broad region on the dayside can propagate into the plasmasphere. After entry into the plasmasphere, waves can propagate eastward in MLT and merge to form hiss. This explains how chorus generated on the dayside can contribute to plasmaspheric hiss in the dusk sector. A subset of waves entering the plasmasphere can even propagate globally onto the nightside. **Citation:** Chen, L., J. Bortnik, R. M. Thorne, R. B. Horne, and V. K. Jordanova (2009), Three-dimensional ray tracing of VLF waves in a magnetospheric environment containing a plasmaspheric plume, *Geophys. Res. Lett.*, *36*, L22101, doi:10.1029/2009GL040451.

## 1. Introduction

[2] Based on detailed ray trace modeling in the noon-midnight meridian plane, *Bortnik et al.* [2008] proposed that plasmaspheric hiss originates from lower-band chorus generated outside the plasmasphere. The day-night asymmetry of hiss was explained as a consequence of weaker Landau damping on the dayside, which allows chorus emissions to propagate to high latitude, where they subsequently migrate onto lower $L$-shells and enter the plasmasphere. Observations on two separate THEMIS spacecraft later confirmed a strong correlation between amplitude modulation of these two distinct waves [*Bortnik et al.*, 2009]. However, these correlated observations of hiss emission and chorus emission were about 3 hours apart in magnetic local time (MLT). Furthermore, earlier statistical analysis of wave data from the Combined Release and Radiation Effects Satellite (CRESS) showed that high latitude lower-band chorus emissions ($4 < L < 7$) are predominately seen on the dayside, over the MLT range between 0600 and 1400 MLT [*Meredith et al.*, 2003]. In contrast, whistler-mode hiss inside the plasmasphere ($2 < L < 4$) is generally found between 0600 and 2100 MLT during active periods, with peak emission in the late afternoon or duskside [*Meredith et al.*, 2004]. More recently, *Li et al.* [2009] analyzed wave magnetic fields on THEMIS and reported that the global distribution of chorus emissions tends to peak in the pre-noon sector at low latitudes.

[3] To validate the idea that plasmaspheric hiss is a result of the evolution of chorus waves that propagate into the plasmasphere, one must account for the distinct difference in the MLT distribution of hiss and chorus. To examine the importance of off-meridian propagation, a three-dimensional ray tracing study is performed. As in previous studies [e.g., *Bortnik et al.*, 2007], we ignore all the aspects of the wave excitation process, and consider only the Landau damping of VLF waves as they propagate away from the their source region near the equator outside the plasmasphere.

## 2. Asymmetrical Density Model

[4] The HOTRAY code [*Horne*, 1989] is used to perform ray tracing in three dimensional space. For this study, an axisymmetric dipole magnetic field is used and a smooth three dimensional density distribution of the storm time magnetosphere is constructed as follows.

[5] 1. The equatorial density distribution is simulated using the plasmaspheric density model of *Rasmussen et al.* [1993] which was developed further to use an arbitrary electric field by *Jordanova et al.* [2006]. In this study the plasmasphere model is driven by the electric field output from Rice Convection model (RCM) for the 2001 April 21st storm. The equatorial density at a specific time during the storm main phase is generated on an $L$-shell grid from 2 to 6.5 every 0.25 and an MLT grid with a grid spacing of 1/2 hour.

[6] 2. The discrete equatorial density is interpolated to generate a smooth equatorial density distribution from $L = 1.2-10$ by using 2-D Hermite interpolation [*Fritsch and Carlson*, 1980; *Phillips*, 1973], which maintains monotonicity in MLT and L in almost every spatial bin. Figure 1b shows in gray scale the typical storm main phase density distribution on the equatorial plane used in our study, which includes a high-density plume in the post-noon sector.

[7] 3. The three dimensional density model is completed, using the latitudinal dependence along the magnetic field lines, given by *Denton et al.* [2002].

## 3. Three-Dimensional Ray Tracing

[8] For the purpose of three dimensional ray tracing, we define the direction of the wave vector **k** in the local Cartesian system as shown in Figure 1a. In this system, the $z$ axis is along the direction of the ambient magnetic field, the $x$ axis is orthogonal to the $z$ axis and lies in the meridian plane pointing away from the Earth at the equator, and the $y$ axis completes the right-handed set. The wave vector **k** makes an angle $\psi$ with the $z$ axis and the projection of **k** onto the $xy$ plane makes

[1]Department of Atmospheric and Oceanic Sciences, University of California, Los Angeles, California, USA.
[2]British Antarctic Survey, Natural Environment Research Council, Cambridge, UK.
[3]ISR-1, Los Alamos National Laboratory, Los Alamos, New Mexico, USA.


0094-8276/09/2009GL040451

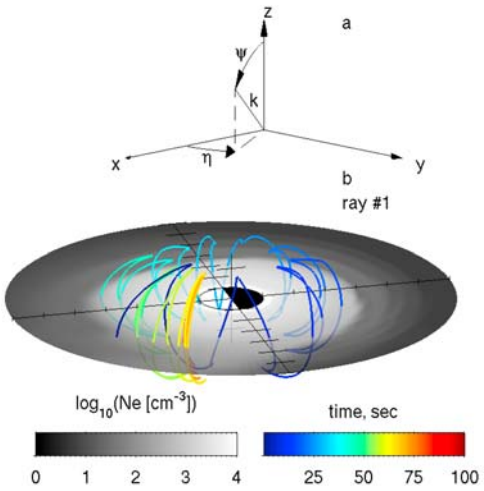


**Figure 1.** (a) Geometry of wave vector **k** in a local coordinate system with z-axis along the direction of the magnetic field. (b) A three dimensional view of the ray path of a whistler-mode wave launched at the equator at $L$ = 5, MLT = 14 with frequency 0.1 $f_{ce}$ (696 Hz), $\psi_0$ = 25°, and $\eta_0$ = 70° (labeled ray 1). Group time $t$ is color-coded along the ray path. The background equatorial thermal electron density is superimposed in gray scale.

an angle $\eta$ with the $x$ axis. $\eta$ = 0°, 90°, 180° and 270° correspond to **k** whose component perpendicular to the ambient magnetic field $\mathbf{k}_\perp$ is directed away from the Earth, toward later MLT (eastward), toward the Earth, and toward earlier MLT (westward), respectively.

[9] Since oblique whistler-mode VLF waves are subjected to Landau damping by electrons of a few keV, a global statistical model of the suprathermal electron population is also constructed using electron fluxes measured by the Low Energy Plasma Analyzer (LEPA) of CRRES over 939 orbits under geomagnetically active conditions (AE > 300 nT). Analytical power law distribution functions are fit to the statistical suprathermal flux observations outside the plasmasphere [e.g., *Bortnik et al.*, 2007], and the model of *Bell et al.* [2002] is used to model suprathermal electron flux inside the plasmapause. The plasmapause location is set to the equatorial density contour of value 50 $cm^{-3}$ in our study. The fitted distribution functions are used to calculate the local Landau damping rate (using Equation (3.9) of *Kennel* [1966]. It should be noted that there is a typo in that equation, i.e., $R$ and $L$ in the fifth line of this equation should be $L$ and $R$ respectively.) The attenuation experienced by a ray is calculated by the local damping rate integrated along the ray path. Ray lifetime is defined as the time when the ray decays to 1% of its initial power.

[10] Figure 1b shows an example of a three dimensional ray path of a whistler mode wave (labeled as ray 1) launched outside the plasmapause near the edge of the plume at $L$ = 5.0 and MLT = 14, with frequency $f$ = 0.1 $f_{ce}$ (696 Hz), initial $\psi_0$ = 25° and $\eta_0$ = 70°, where $f_{ce}$ is the ambient electron gyrofrequency. Propagation characteristics of this ray are also shown in Figure 2a. The ray propagates outside the plasmasphere for less than 1 second, where most of the Landau damping occurs, and then enters the plasmasphere, where the ray decays much more slowly due to lower suprathermal electron flux. The ray is trapped inside the plasmasphere, propagates across the entire range of MLT, and experiences repeated magnetospheric reflection and plasmapause bouncing until it enters the plume again at $t \sim$ 50 seconds. Magnetospheric reflection is characterized by a passage of $\psi$ through 90°, during which the wave can reverse the component of its group velocity along the ambient magnetic field. Plasmapause bouncing occurs, according to Snell's law, at the steep density region near the plasmapause. This feature is indicated by the spikes along the upper envelope of the $L$-shell evolution profile (Figure 2b), taking place at different $L$s at different MLTs because of the asymmetry of the plasmasphere. Eventually the ray becomes trapped within the plume, exhibiting only magnetospheric reflections in the meridian plane near MLT = 15.5 due to lack of a steep density gradients, which are required for plasmapause bouncing. The attenuation rate is a little slower during the early phase when plasmapause bouncing occurs, $t$ < 50 seconds (Figure 2d), primarily because plasmapause bouncing keeps the wave normal angle $\psi$ more field-aligned.

[11] Figure 2 also shows the propagation characteristics of two other rays, labeled ray 2 and 3, launched from the same source location, but with different initial propagation angles. Ray 2 (with $\psi_0$ = 31° and $\eta_0$ = 180°) experiences strong Landau damping to 50% of the initial power at $t$ = 0.2 second and then enters the plasmasphere. During the following 10 seconds, this ray also propagates across 3 hours in MLT into the plume region. Soon after that, the ray eventually

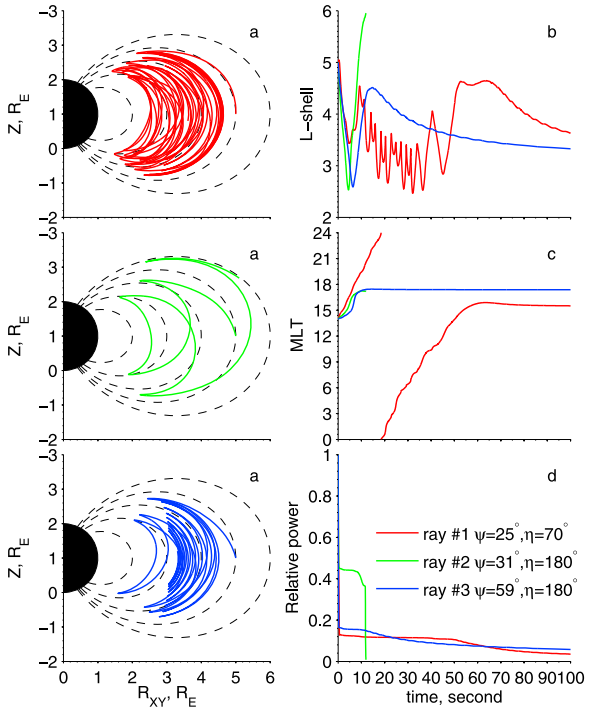


**Figure 2.** Propagation characteristics of waves launched at the same equatorial location $L$ = 5 and MLT = 14, with the same frequency (0.1 $f_{ce}$) but different initial wave vector directions. (a) Z versus $R_{XY}$ (= $\sqrt{X^2 + Y^2}$) for rays (top) 1, (middle) 2, and (bottom) 3; (b) L versus group time $t$; (c) MLT versus group time $t$; and (d) relative power versus group time $t$.

damps out when it escapes from the plasmasphere (Figures 2b and 2d). Ray 3 (with $\psi_0 = 59^\circ$ and $\eta_0 = 180^\circ$) also propagates into the plume and eventually migrates toward smaller $L$, due to multiple magnetosphere reflections inside the plume near MLT $\approx$ 17. This ray survives for over 100 seconds because of lower the damping rate in the high-density regions. These rays (1, 2, and 3) shows three representative, but different, types of ray trajectories: global propagation, escaping from the plume or plasmasphere, and plume trapping.

[12] The single ray trajectories illustrated in Figure 2 have been repeated multiple times, in each case varying one of initial parameters (e.g., $L$, MLT, $f$, $\psi$, $\eta$). For this initial study, we fix the source region at $L = 5$, and frequency $f = 696$ Hz (0.1 $f_{ce}$) and perform 3-D ray-tracing for whistler-mode waves with different initial MLT, $\psi_0$ and $\eta_0$. Figure 3 shows the equatorial projection of each ray path along $L$-shells (left column) and life time (right column) of each ray as a function of initial $\psi_0$ and $\eta_0$, parameterized into 4 rows representing different initial MLT (6, 10, 12, 14 hours from the top to the bottom). The thermal electron density distribution is superimposed on the left column in gray scale with white color representing the region where density is greater than 50 cm$^{-3}$, used to define entry into the plasmasphere in this study. The colored lines in Figures 3a, 3c, 3e, and 3g are ray paths projected onto the equatorial plane for waves with 33 values of $\psi_0$ from 1° to 65° at 2° spacing and 72 values of $\eta_0$ equally spaced over 360°, consistent with a broad range of wave normals observed in the chorus source region [*Breneman et al.*, 2009]. The colors of these lines represents different values of $\psi_0$; lines with the same $\psi_0$ but different $\eta_0$ are plotted in the same color. For rays launched at MLT = 6 (Figures 3a and 3b), all rays remain outside the plasmasphere, and damp out in less than 0.4 seconds as they propagate toward high latitude due to strong damping in the dawn sector. A similar behavior occurs at this $L$-shell throughout the entire night sector (not shown here). For rays launched at MLT = 10, those rays with high wave normal angle $\psi_0$ (>60°) and $\mathbf{k}_\perp$ pointing toward the Earth and slightly eastward ($135^\circ < \eta_0 < 180^\circ$) can penetrate into the plasmasphere and endure for over 100 seconds. All of these rays propagate eastward, due to steep eastward density gradient at MLT $\approx$ 10, and migrate across about 5 hours in MLT on average inside the plasmasphere. Other rays confined outside the plasmasphere generally also propagate across 1 or 2 hours in MLT, but survive for less than 2 seconds. For rays initiated in the noon sector (Figures 3e and 3f), entry into the plasmasphere is greatly enhanced, due to the extended plasmapause location and less suprathermal electron flux, and extends to smaller $\psi_0$ (>35°) and a broader range of $\eta_0$ centered at $\eta_0 = 180^\circ$. Those rays that enter the plasmasphere are able to propagate in both eastward and westward directions, since the density gradient associated with the plasmapause is almost radial at MLT = 12. Most rays launched at MLT = 14 (Figures 3g and 3h) are pulled toward the higher density, even those with initial $\mathbf{k}$ pointing westward, and subsequently propagate eastward because of the steep eastward density gradient associated with the early-MLT edge of the plume. A few rays can bounce back toward the west inside the plasmasphere from eastward propagation after several plasmapause bounces, due to the asymmetry of plasmapause shape during storm conditions.

[13] A variety of interesting propagation characteristics occur for chorus waves launched at 1400 MLT (Figures 3g and 3h) near the edge of the plume, which basically fall into four different categories:

[14] 1. rays with lifetime less than 1 second launched with $-60^\circ < \eta_0 < 60^\circ$ and $\psi_0 > 20^\circ$ ($\mathbf{k}$ directed away from the Earth); Such rays are confined to the region outside the plasmasphere and damp out within less than a few seconds. They also tend to propagate eastward, indicated by a much higher density of ray paths to the east of the launch point (Figure 3g).

[15] 2. rays with a lifetime of over one hundred seconds with wave vectors pointing toward the Earth with $\psi_0 > 50^\circ$ or with wave vectors pointing westward with any $\psi_0$, even as low as $\psi_0 = 0$ (field aligned); These rays (like ray 3 in Figure 2) can enter the plasmasphere and propagate westward until they reach the plume. Subsequently, the rays become trapped inside the high density plume in the meridian plane at a certain MLT, exhibit multiple magnetospheric reflections and migrate toward smaller $L$-shells.

[16] 3. rays with a lifetime of about 100 seconds or more with wave vector directed toward the plume (eastward); This type of ray (like ray 1 in Figure 2) can jump over the plume and exhibit large migration in MLT, and even global propagation over all MLT. This type of ray, from a single location with single frequency but a range of wave vector directions, can eventually fill the whole plasmasphere, including the nightside.

[17] 4. rays with a lifetime of about 10 seconds with $\psi_0 < 20^\circ$ pointing westward, or $30 < \psi_0 < 50$ toward the Earth; Such rays (like ray 2 in Figure 2) are pulled into the plume and then escape toward larger $L$ inside the plume, thus becoming damped more quickly than the rays of the second type.

## 4. Principal Findings and Future Study

[18] This initial three dimensional ray tracing study of VLF waves has revealed a variety of new propagation characteristics, which are important for understanding the origin of plasmaspheric hiss:

[19] 1. VLF chorus excited near the equator on the dayside can propagate to high latitude and enter the plasmasphere from a broad range of MLT source locations. The ability to access the plasmasphere depends on the distance of the plasmapause from the wave source region, and the initial wave normal direction of emitted waves.

[20] 2. VLF waves can propagate azimuthally both inside and outside the plasmasphere. However, pronounced off-meridian propagation is most effective in the post-noon sector, due to the weaker Landau damping rate and larger azimuthal density gradients. Off-meridian propagation also becomes more effective inside the plasmasphere than outside, due to internal ray reflection from the plasmapause. Plasmapause reflections enable large MLT transport, even globally across all MLT, and such waves may transit from eastward propagation to westward propagation or vice verse because of plasmapause asymmetry.

[21] 3. VLF waves that propagate into the plasmaspheric plume tend to remain confined inside the plume, exhibiting magnetospheric reflections with no plasmapause reflection due to the lack of a steep density gradient. Such confinement

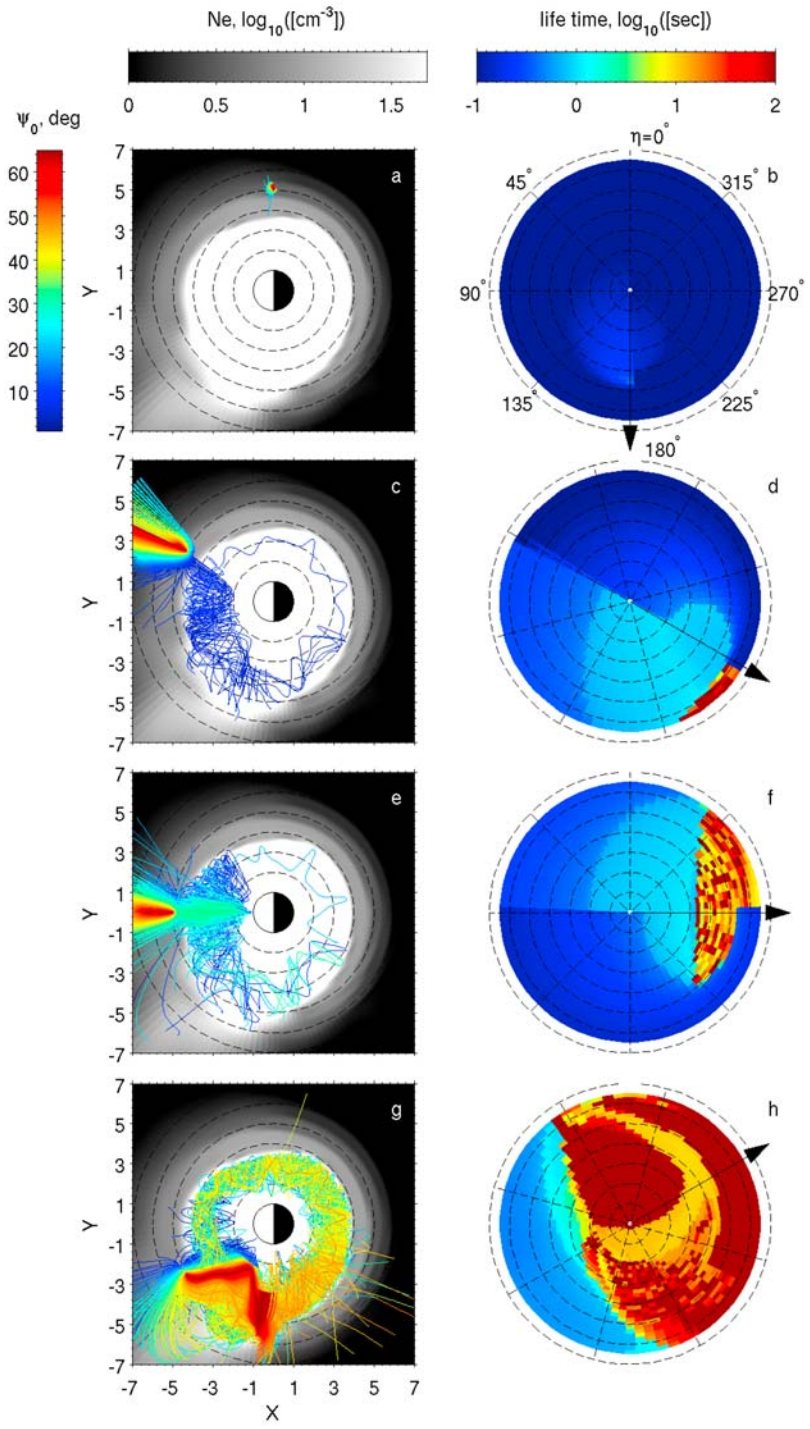


**Figure 3.** (left) Superposition of ray paths mapped onto the equatorial plane along field lines for whistler-mode waves with the same frequency (0.1 $f_{ce}$) but varying directions of waves vectors, launched from the equatorial plane at $L = 5$ and MLT = (a–b) 6, (c–d) 10, (e–f) 12, and (g–h) 14. The 33 values of $\psi_0$ (color-coded) are illustrated from 1° to 65° with 2° spacing and 72 values of $\eta_0$ from 0° to 355° with 5° spacing. Thermal plasma density is shown in gray scale. (right) Corresponding life time as a function of $\psi_0$ and $\eta_0$. Seven dashed circles represent $\psi_0$ from 10 ° and 70° with 10° apart. The arrow represents the direction to the Earth, i.e., denoting the direction **k** with $\eta_0 = 180°$.

is consistent with intense VLF emission observed on the duskside during storm times [*Thorne et al.*, 1974; *Summers et al.*, 2008].

[22] The initial investigation of the role of azimuthal density gradient on the ray path of VLF waves was performed for a specific density model appropriate during the main phase of a storm. Nonetheless, we anticipate that some of the general features of wave access into the plasmasphere should also be present for any non-axisymmetric density distribution. This can be explored in 3D ray tracing studies with a

variety of different global density models. In future we plan to follow the 3D ray paths of chorus emissions from a range of source $L$ values and at different frequencies, and investigate whether this can account for the spatial distribution and spectral properties of plasmaspheric hiss.

[23] **Acknowledgments.** This research was supported by the NASA grants NNX08A135G and NNH08AJ01I.

## References

Bell, T. F., U. S. Inan, J. Bortnik, and J. D. Scudder (2002), The Landau damping of magnetospherically reflected whistlers within the plasmasphere, *Geophys. Res. Lett.*, *29*(15), 1733, doi:10.1029/2002GL014752.

Bortnik, J., R. M. Thorne, and N. P. Meredith (2007), Modeling the propagation characteristics of chorus using CRRES suprathermal electron fluxes, *J. Geophys. Res.*, *112*, A08204, doi:10.1029/2006JA012237.

Bortnik, J., R. M. Thorne, and N. P. Meredith (2008), The unexpected origin of plasmaspheric hiss from discrete chorus emissions, *Nature*, *452*, 62–66.

Bortnik, J., W. Li, R. M. Thorne, V. Angelopoulos, C. Cully, J. Bonnell, O. Le Contel, and A. Roux (2009), An observation linking the origin of plasmaspheric hiss to discrete chorus emissions, *Science*, *324*, 775–778, doi:10.1126/science.1171273.

Breneman, A. W., C. A. Kletzing, J. Pickett, J. Chum, and O. Santolik (2009), Statistics of multispacecraft observations of chorus dispersion and source location, *J. Geophys. Res.*, *114*, A06202, doi:10.1029/2008JA013549.

Denton, R. E., J. Goldstein, and J. D. Menietti (2002), Field line dependence of magnetospheric electron density, *Geophys. Res. Lett.*, *29*(24), 2205, doi:10.1029/2002GL015963.

Fritsch, F. N., and R. E. Carlson (1980), Monotone piecewise cubic interpolation, *SIAM J. Numer. Anal.*, *17*, 238–246, doi:10.1137/0717021.

Horne, R. B. (1989), Path-integrated growth of electrostatic waves: The generation of terrestrial myriametric radiation, *J. Geophys. Res.*, *94*, 8895–8909.

Jordanova, V. K., Y. S. Miyoshi, S. Zaharia, M. F. Thomsen, G. D. Reeves, D. S. Evans, C. G. Mouikis, and J. F. Fennell (2006), Kinetic simulations of ring current evolution during the Geospace Environment Modeling challenge events, *J. Geophys. Res.*, *111*, A11S10, doi:10.1029/2006JA011644.

Kennel, C. (1966), Low-frequency whistler mode, *Phys. Fluids*, *9*, 2190–2202, doi:10.1063/1.1761588.

Li, W., R. M. Thorne, V. Angelopoulos, J. Bortnik, C. M. Cully, B. Ni, O. LeContel, A. Roux, U. Auster, and W. Magnes (2009), Global distribution of whistler-mode chorus waves observed on the THEMIS spacecraft, *Geophys. Res. Lett.*, *36*, L09104, doi:10.1029/2009GL037595.

Meredith, N. P., R. B. Horne, R. M. Thorne, and R. R. Anderson (2003), Favored regions for chorus-driven electron acceleration to relativistic energies in the Earth's outer radiation belt, *Geophys. Res. Lett.*, *30*(16), 1871, doi:10.1029/2003GL017698.

Meredith, N. P., R. B. Horne, R. M. Thorne, D. Summers, and R. R. Anderson (2004), Substorm dependence of plasmaspheric hiss, *J. Geophys. Res.*, *109*, A06209, doi:10.1029/2004JA010387.

Phillips, G. M. (1973), Explicit forms for certain Hermite approximations, *BIT Numer. Math.*, *13*, 177–180.

Rasmussen, C. E., S. M. Guiter, and S. G. Thomas (1993), A two-dimensional model of the plasmasphere: Refilling time constants, *Planet. Space Sci.*, *41*, 35–43, doi:10.1016/0032-0633(93)90015-T.

Summers, D., B. Ni, N. P. Meredith, R. B. Horne, R. M. Thorne, M. B. Moldwin, and R. R. Anderson (2008), Electron scattering by whistler-mode ELF hiss in plasmaspheric plumes, *J. Geophys. Res.*, *113*, A04219, doi:10.1029/2007JA012678.

Thorne, R. M., E. J. Smith, K. J. Fiske, and S. R. Church (1974), Intensity variation of ELF hiss and chorus during isolated substorms, *Geophys. Res. Lett.*, *1*, 193–196, doi:10.1029/GL001i005p00193.

J. Bortnik, L. Chen, and R. M. Thorne, Department of Atmospheric and Oceanic Sciences, University of California, Los Angeles, CA 90024, USA. (clj@atmos.ucla.edu)

R. B. Horne, British Antarctic Survey, Natural Environment Research Council, Madingley Rd., Cambridge CB3 0ET, UK.

V. K. Jordanova, ISR-1, MS D466, Los Alamos National Laboratory, Los Alamos, NM 87545, USA.